Biophysical Journal
Article

Biophysical Society

Core-Shell Modeling of Light Scattering by Vesicles: Effect of Size, Contents, and Lamellarity

Anna Wang,[1,*] Christopher Chan Miller,[2] and Jack W. Szostak[1,*]
[1]Department of Molecular Biology and Center for Computational and Integrative Biology, Massachusetts General Hospital, Boston, Massachusetts and [2]Atomic and Molecular Physics Division, Harvard Smithsonian Center for Astrophysics, Cambridge, Massachusetts

ABSTRACT Having a fast, reliable method for characterizing vesicles is vital for their use as model cell membranes in biophysics, synthetic biology, and origins of life studies. Instead of the traditionally used Rayleigh-Gans-Debye approximation, we use an exact extended Lorenz-Mie solution for how core-shell particles scatter light to model vesicle turbidity. This approach enables accurate interpretations of simple turbidimetric measurements and is able to accurately model highly scattering vesicles, such as larger vesicles, those with multiple layers, and those with encapsulated material. We uncover several surprising features, including that vesicle lamellarity has a larger effect on sample turbidity than vesicle size and that the technique can be used to measure the membrane thickness of vesicles. We also examine potential misinterpretations of turbidimetry and discuss when measurements are limited by forward and multiple scattering and by the geometry of the instrument.

INTRODUCTION

The desire to characterize and monitor the properties of vesicles—semipermeable membranes that enclose an aqueous compartment (Fig. 1 *A*)—comes from many fields. Vesicles can be biocompatible and deliver cargo for drug delivery (1,2), are used as compartments for synthetic biology (3) and origins of life studies (4), and are used as model systems to study cell-membrane properties (5). A noninvasive way to determine the properties of vesicles is to use their interaction with visible light. For example, static and dynamic light scattering (DLS) is often used for vesicle sizing (6), microscopy is used to determine morphologies of vesicles (7), multiangle light scattering is used to size vesicles (8) and during flow cytometry to distinguish between cell types (9), and fluorescence measurements are routinely used to assess vesicle encapsulation efficiency (10).

One commonly used optical technique is turbidimetry (Fig. 1 *B*), in which the turbidity of a sample is measured using the widely available spectrophotometer. Researchers have used this technique to assess a variety of vesicle properties, including vesicle formation (11–13), dissolution (14), permeability (15), flocculation (16), average vesicle size (17–20), membrane bilayer thickness (21), and change in average vesicle size (22). Changes in turbidity are usually attributed to just a single parameter, even though the turbidity of a sample depends on all of these quantities.

It is precisely the versatility of turbidimetry that begs the following question: if the turbidity of a sample increases or decreases, how is it possible to determine which vesicle property is causing the change? Some studies invoke light-scattering theory to calculate the scattering properties of individual vesicles—their scattering cross section and efficiencies—to help tease apart these effects. Most studies use the Rayleigh-Gans-Debye approximation (17,18,21) in part because it has an analytical form and in part because many of these calculations were done before the availability of adequate computational power (23). Although the error in the calculated scattering efficiency can be as low as 1% for some vesicle sizes (24), the approximation breaks down when vesicles encapsulate materials that differ from the outside or when vesicles have multiple bilayers, otherwise known as multilamellar vesicles (Fig. 1 *A*).

Here, we circumvent these limitations by using a numerically stable multilayered-sphere light-scattering solution (25,26) that explicitly specifies the bilayers and interbilayer spaces to calculate how vesicles scatter light. Because the exact Lorenz-Mie solution for spheres was extended to core-shell spheres more than half a century ago (27), there have been many improvements on algorithms and

Submitted July 18, 2018, and accepted for publication January 2, 2019.

*Correspondence: anna.wang@unsw.edu.au or szostak@molbio.mgh.harvard.edu

Anna Wang's present address is School of Chemistry, University of New South Wales Sydney, Kensington, New South Wales, Australia.

Editor: Arne Gericke.

https://doi.org/10.1016/j.bpj.2019.01.006

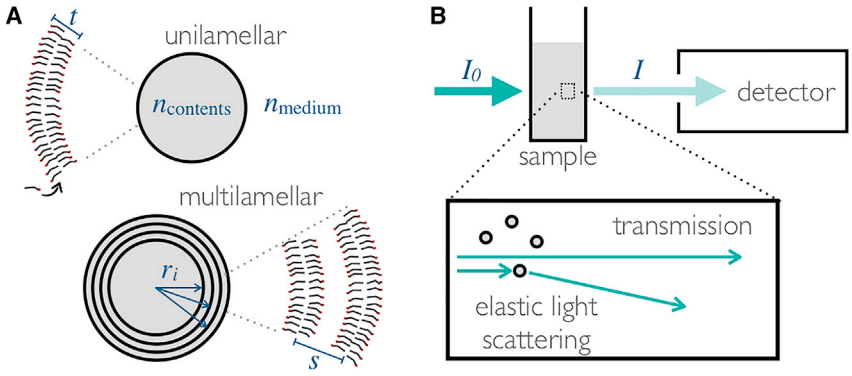

FIGURE 1 (*A*) Vesicles are semipermeable compartments delineated by a membrane. The membrane is typically a bilayer of amphiphile and encloses a material of refractive index $n_{contents}$ in a medium of refractive index n_{medium}. Unilamellar vesicles have one membrane of thickness t, and multilamellar vesicles have many membranes with center-to-center separations s. (*B*) The turbidity of vesicle samples can be measured on a spectrophotometer. The detector measures the intensity of light I that passes 180° through a sample with an illumination source of intensity I_0. This is typically a measure of how much light is unattenuated (transmitted). To see this figure in color, go online.

computational power (28) to make the solution usable. Although the near-field solution requires further refining (29), in the far field, extended Lorenz-Mie core-shell models are now commonly used by atmospheric scientists to study aerosols such as soot coated with water (30) and by photonics researchers to study the optical properties of core-shell nanoparticles (31,32). Here, we apply this approach to the study of vesicles. Because the model is based on the exact Lorenz-Mie solution, it can handle encapsulated contents, multilamellarity, and larger scatterers than the Rayleigh-Gans-Debye approximation.

We find that a change in turbidity can easily be misattributed to the incorrect parameter. For example, a sample of bilamellar vesicles has the same turbidity (across all wavelengths) as a unilamellar sample with twice the concentration. We show how sample turbidity depends on vesicle size, composition, contents, and lamellarity. We also determine when forward scattering, multiple scattering, and instrument geometry need to be taken into account to interpret the measurements in a quantitative manner.

Finally, we fit our model to turbidity measurements made on a spectrophotometer to measure the membrane thickness of oleic acid vesicles and POPC vesicles to excellent agreement with the literature, demonstrating that when used in conjunction with DLS, optical microscopy, and light-scattering calculations, turbidimetry can be a quantitative and powerful tool.

MATERIALS AND METHODS

To make fatty acid vesicles, we first made micelles by dissolving 200 μmol of neat fatty acid oil—oleic acid, palmitoleic acid, or myristoleic acid (Nu-Chek Prep, Waterville, MN)—in 1.25 equivalents of NaOH (Sigma-Aldrich, St. Louis, MO). The solution was then brought to a volume of 2 mL with Millipore (Burlington, MA) water (18.2 M cmΩ), vortexed, and left on a test-tube rocker (Speci-Mix, Thermo Fisher Scientific, Waltham, MA) for at least 1 h to yield a 100 mM solution. The concentrated buffer stock (0.5 M) was made by dissolving bicine (Sigma-Aldrich) in Millipore water (18.2 M cmΩ) and then titrating the solution to the desired pH with NaOH (Sigma-Aldrich). We made vesicles by mixing the micelle solution, buffer stock, and Millipore water to the desired final concentration in a microcentrifuge tube, vortexing for 5 s, and then leaving the sample to agitate overnight on an orbital shaker (GeneMate, BioExpress, Kaysville, UT). All fatty acid vesicle samples were made with 200 mM bicine, except for giant oligolamellar vesicles, which were made with 50 mM bicine. To make phospholipid vesicles, we deposited 30 μL of a 25 mg/mL solution of 1-palmitoyl-2-oleoyl-sn-glycero-3-phosphocholine (POPC) in chloroform (Avanti Polar Lipids, Alabaster, AL) into a glass vial, evaporated the chloroform under a stream of nitrogen, and hydrated the POPC film with 1 mL of 200 mM bicine buffer. The extruded samples were prepared with a miniextruder (Avanti Polar Lipids) through a Whatman Nuclepore polycarbonate filter with 50-nm-diameter pores 11 times and left to tumble on a tube rotator (Labquake, Thermo Fisher Scientific) for at least 1 h before making any measurements.

Turbidity was measured on a spectrophotometer (Cary 60; Agilent, Santa Clara, CA). A solution containing just the buffer was used as the blank. The vesicle size distribution was measured with DLS on a Zetasizer Nano C (Malvern Panalytical, Malvern, U.K.). Samples were held in ultraviolet cuvettes (BRAND GMBH + CO KG, Wertheim, Germany). Refractive indices of solutions at 589 nm, without vesicles present, were measured on an Abbe refractometer (C10 VEE GEE, VEE GEE Scientific, Kirkland, WA) at 22°C. Glucose, sucrose, and adenosine 5′-monophosphate disodium salt ($\geq$99%) were all obtained from Sigma-Aldrich. Concentrations of RNA were determined by spectrophotometry on a Nanodrop 2000C (Thermo Fisher Scientific).

Radiative transfer calculations were done using the solution to the Eddington approximation taken directly from Shettle and Weinman (33), incorporating the δ-Eddington approximation from Joseph et al. (34). The aperture was assumed to be completely nonreflecting.

Defining turbidity

Before proceeding, we first seek to unambiguously relate how individual vesicles scatter light to the measured turbidity of a vesicle sample. In general, there are three main outcomes for a photon as it encounters a vesicle (Fig. 1): It can pass by without interacting (be transmitted), be absorbed (for example, by a fluorophore or a dye), or elastically scatter off the vesicle without changing its wavelength (35). Once a photon passes through an entire sample, there are analogous quantities that describe the effect of the whole sample on light. The extinction ε refers to the attenuation of photons as they pass through a sample and consists of the attenuation owing to absorption (absorbance A) and the attenuation owing to scattering ($\mathcal{T}$).

It has long been proposed that spectrophotometers can be used to measure not just the absorbance of absorbing samples but also the turbidity of nonabsorbing samples (17). This is because although spectrophotometers report an "absorbance" A, the quantity that is actually measured is how much light does not make it through the sample toward a detector situated opposite from the light source (see Fig. 1 *B*): the extinction ε. Thus, a typical spectrophotometer reports an "absorbance"

$$\text{Abs} = -\log_{10}(I/I_0) = \varepsilon = A + \mathcal{T}, \qquad (1)$$

where I_0 is the incident light intensity, I is the intensity of light that enters the detector, and $\mathcal{T}$ is the extinction owing to scattering. It is assumed that no light is scattered into the detector. We will revisit this assumption in the section examining the effects of scattering toward the detector.

For absorbing samples that have insignificant light scattering ($\mathcal{T} = 0$), the measured quantity ε equals a true absorbance A, and the concentration of a sample can be determined by using $A = \varepsilon_A cl$, otherwise known as the Beer-Lambert law. Here, ε_A is the molar absorption coefficient ($[\varepsilon_A] = \mathrm{M}^{-1}\ \mathrm{cm}^{-1}$), c is the concentration of the absorbing molecule ($[c]$ moles/L = M), and l is the path length (usually through a cuvette, $l \sim 1$ cm).

When describing nonabsorbing samples, the total attenuation of light after it passes through a sample is usually described by a turbidity or optical depth τ:

$$\tau = -\ln(I/I_0) = \sigma_{\mathrm{sca}} N l, \tag{2}$$

assuming the fraction of light scattered in the direction of the detector is insignificant. σ_{sca} is the scattering cross section per scatterer (e.g., a vesicle, $[\sigma_{\mathrm{sca}}] = \mathrm{m}^2$), and N is the number density of scatterers ($[N] = \mathrm{m}^{-3}$). By Eqs. 1 and 2, the turbidity of a nonabsorbing sample ($A = 0$) can be measured on a spectrophotometer; the "absorption" ε measured on spectrophotometers is in fact linearly proportional to the turbidity $\tau \sim 2.3\varepsilon = 2.3\mathcal{T}$.

For a concentration c ($[c] = \mathrm{mol/L}$) of amphiphile in a system, the number density of vesicles N ($[N] = \mathrm{m}^{-3}$) can be rewritten as

$$N = 10^3 c N_A / \ell = 10^3 c N_A (a_v/a)^{-1}, \tag{3}$$

where N_A is Avogadro's number, ℓ is the number of amphiphile molecules per vesicle, a is the area per amphiphile in a membrane, and total leaflet area is $a_v = \sum_i 8\pi r_i^2$, where r_i is the radius of each of the q membranes in the vesicle (measured from the center of the vesicle to the middle of the membrane). The factor of 1000 is present because of the difference in volume units between number density N (m^{-3}) and concentration c (mol/L). The turbidity from Eq. 2 then becomes

$$\tau = \sigma_{\mathrm{sca}} N l = 10^3 c N_A a l \sigma_{\mathrm{sca}} / a_v. \tag{4}$$

Because the turbidity scales linearly with the concentration of amphiphile c and the path length l, we can also define the molar turbidity coefficient $\varepsilon_\tau = \tau/cl = 10^3 N_A a \sigma_{scd}/a_v$, which has units $\mathrm{M}^{-1}\ \mathrm{cm}^{-1}$ analogous to the molar absorption coefficient ε_A in Eq. 1.

For absorbing samples, we can replace σ_{sca} with the absorption cross section σ_{abs} in Eq. 4 and find the absorbance A_e (related to the absorbance as measured on a spectrophotometer, $A \sim 2.3A_e$):

$$A_e = \sigma_{\mathrm{abs}} N l = 10^3 c N_A a l \sigma_{\mathrm{abs}} / a_v. \tag{5}$$

We calculate the scattering cross section σ_{sca} and the absorption cross section σ_{abs} with Yang's recursive algorithm within the light-scattering package HoloPy. HoloPy is open source and can be found at https://github.com/manoharan-lab/holopy. Examples of how to use HoloPy to calculate vesicle scattering cross sections can be found at https://github.com/anna-wang/vesicle-turbidity. Although this algorithm can calculate cross sections for vesicles with an arbitrary number of layers of arbitrary thicknesses, the layers must be concentric. The scattering and absorption cross sections of arbitrary scatterers can be calculated in HoloPy with an implementation of the discrete dipole algorithm (36,37). Eqs. 4 and 5 are then used to calculate τ and A.

For core-shell structures such as vesicles, the scattering cross section depends on the set of parameters

$$\{p\} = \left\{r_{1,\ldots,q}, n_{\mathrm{contents}}, n_{\mathrm{medium}}, t, n_{\mathrm{membrane}}\right\}, \tag{6}$$

where n_{contents} is the content refractive index, n_{medium} is the external solution refractive index, t is the membrane thickness, and n_{membrane} is the membrane refractive index. In this work, we do not consider vesicles with nonconcentric centers or uneven spacing. We assume a spherical geometry and that the membranes are evenly spaced with s being the center-to-center spacing between membranes. We define the radius of the vesicle r as the distance between the vesicle center and the center of the outermost membrane.

RESULTS

For simplicity and ease of comparison to experiments, we report calculated turbidities τ and absorbances A for samples with 5 mM total membrane lipid and a path length of 1 cm unless stated otherwise. The lipid parameters we use are that of a lipid similar to oleic acid, with $n_{\mathrm{membrane}} = 1.46$, $t = 3.2$ nm, and $a = 0.311\ \mathrm{nm}^2$ taken from Han (38).

Vesicle size

We begin by checking the intuition that as the vesicle size in a sample increases, so does the sample turbidity. We find that for vesicles in which the contents have no refractive index contrast with the medium $n_{\mathrm{contents}} = n_{\mathrm{medium}}$, the turbidity of the system increases roughly with the logarithm of vesicle size for a fixed total concentration of lipid in the sample (Fig. 2).

Membrane properties: Thickness and refractive index

We now consider how the optical properties of the membrane—its thickness and refractive index—affect the sample turbidity.

We find that increasing the membrane thickness and refractive index increases the sample turbidity (Fig. 3 *A*) and that these curves collapse into a straight line when plotted against the square of the optical path difference $t\Delta n$ (Fig. 3 *B*). One consequence of this result is that the two parameters t and n cannot independently be determined using turbidity alone.

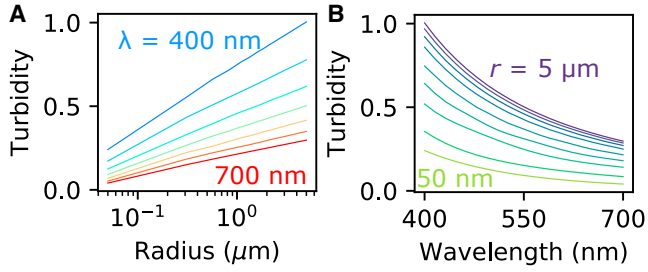

FIGURE 2 Turbidity of a 5 mM sample of vesicles as a function of (*A*). The vesicle radius ($\lambda = 400$, 450, 500, 550, 600, 650, and 700 nm) and (*B*) wavelength ($r = 50$, 100, 250, and 500 nm and 1, 2, 3, 4, and 5 μm) are shown. To see this figure in color, go online.

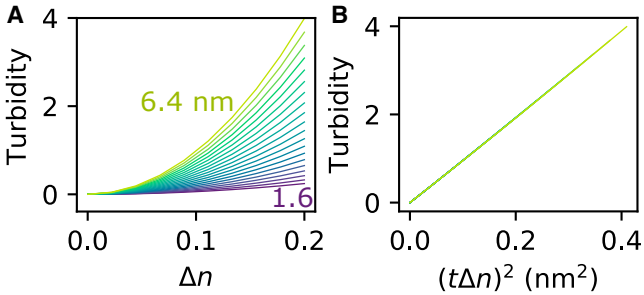

FIGURE 3 (*A*) Calculated turbidity of 5 mM samples of 100-nm-diameter vesicles of increasing membrane thickness t. $\lambda = 400$ nm. (*B*) The calculated turbidity collapses onto a single line when plotted against $(t\Delta n)^2$. $\lambda = 400$ nm. To see this figure in color, go online.

Encapsulated content refractive index

Next, we consider the effect of any encapsulated solutes on vesicle scattering. Experimentalists routinely use purification methods, such as size exclusion chromatography (39,40) or dialysis (41), to remove unwanted solutes that are not encapsulated inside vesicles. Sometimes these solutes are nonabsorbing, such as salts, and contribute to the real part of the refractive index $\mathrm{Re}(n_{\mathrm{contents}})$; other times, they absorb light and contribute to the imaginary part of the refractive index $\mathrm{Im}(n_{\mathrm{contents}}) = k$. Here, for simplicity, we assume that the medium is nonabsorbing, $\mathrm{Im}(n_{\mathrm{medium}}) = 0$, and do calculations at one wavelength ($\lambda = 400$ nm). Both real and imaginary parts of the refractive index usually vary with wavelength. The wavelength dependence of k can be used to separate the effects of absorbance and turbidity (42).

For vesicles that encapsulate a nonabsorbing solution that has a different refractive index from the surrounding medium ($\Delta n_{io} \neq 0$), the turbidity of the sample increases nonlinearly with the vesicle radius (Fig. 4 *A*). This scaling is in contrast to vesicles in which $n_{\mathrm{contents}} = n_{\mathrm{medium}}$ (Fig. 2). Because the surface area/volume ratio of the vesicles decreases with increasing vesicle size, the contribution of even a small $\Delta n_{\mathrm{io}} = n_{\mathrm{contents}} - n_{\mathrm{medium}}$ to sample turbidity can easily surpass that of the membrane for larger vesicles. By measuring the refractive indices of various solutions, we find that the typical values of Δn_{io} in samples that could have enhanced turbidity from content scattering are 0.0025 for vesicles with 100 mM encapsulated sucrose and 100 mM glucose in the external aqueous phase, 0.001 for 15 mM encapsulated adenosine 5′-monophosphate (disodium salt), and 0.001–0.002 for 1 mM encapsulated 12–16 long RNA sequences (see Materials and Methods). These differences in refractive index would significantly affect turbidity (>20% enhancement) for vesicles of radius greater than 50 nm for $\Delta n_{\mathrm{io}} = 0.0025$ and 100 nm for $\Delta n_{\mathrm{io}} = 0.001$.

Using Eq. 5, we find that for vesicles encapsulating a solution that absorbs light ($k \neq 0$ at wavelength λ^*), such as a dye, the absorbance of the sample increases linearly with

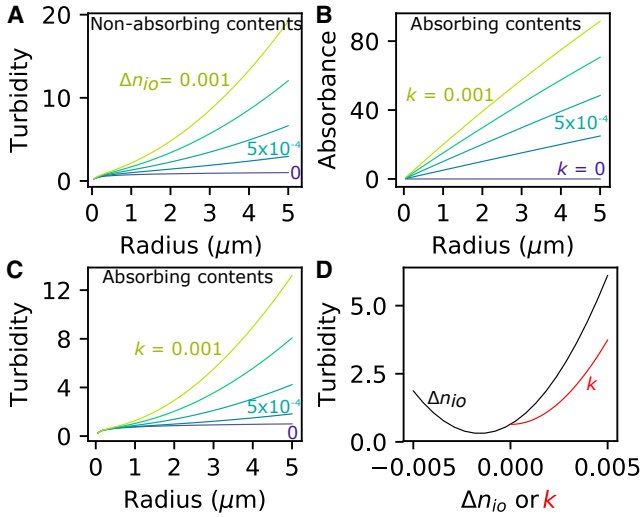

FIGURE 4 (*A*) The turbidity of a nonabsorbing sample increases with the refractive index contrast (Δn_{io}) between the inside and the outside of the vesicles. $\lambda = 400$ nm. (*B*) The absorbance A of a 5 mM sample of vesicles encapsulating an absorbing material (such as a dye) increases with vesicle radius and k. $\lambda = \lambda^* = 400$ nm. (*C*) The turbidity of a 5 mM sample of vesicles encapsulating an absorbing material (such as a dye) increases with vesicle radius and k ($\lambda = \lambda^* = 400$ nm). (*D*) The turbidity of a 5 mM sample of vesicles increases when either the real or imaginary parts of the refractive index of the contents differ from the refractive index of the medium. $\lambda = 400$ nm, $r = 500$ nm. To see this figure in color, go online.

vesicle radius when the total concentration of lipid in the sample is fixed (Fig. 4 *B*). This is because, assuming negligible scattering, the absorbance of the sample increases linearly with the number of absorbing molecules in the sample (Beer's law), and when the total lipid concentration in a sample is fixed, the encapsulated volume increases linearly with the radius (whereas the number of vesicles decreases).

Interestingly, for large enough k, encapsulating an absorbing solution can also enhance the sample turbidity (Fig. 4 *C*) at the wavelengths for which light is absorbed. The measurement for A on a spectrophotometer at λ^* can therefore be affected by ε_τ, although the magnitude of the effect is complex and depends on the exact conditions (43). In general, a change in the imaginary part of the refractive index affects the real part of the refractive index by the Kramers-Kronig relation (44). We expect this effect to be pronounced for vesicles encapsulating a very high concentration of dye, such as self-quenching concentrations of calcein (~100 mM), when monitoring dye leakage. We estimate that k at the absorption maximal wavelength is ~0.0007 for 1 mM calcein and 0.02 for 1 mM phycoerythrin by comparing Eq. 1 to molar extinction coefficients (45).

In general, the effect of any refractive index mismatch between the encapsulated contents and medium will contribute to sample turbidity (Fig. 4 *D*). The extremely large sample turbidities or absorbances calculated by our model indicate scenarios in which any attempt to make a measurement is severely limited by the amount of light transmitted (just

1% of light for Abs = 2 or $A_e \sim 4.6$ or $\tau \sim 4.6$). Caution must therefore be exercised when attempting to make turbidity measurements of samples with encapsulated contents. Interestingly, the sample turbidity can also be decreased by an index mixmatch if a lower content index compensates for the higher index membrane.

Vesicle lamellarity

Thus far, we have only considered scattering from unilamellar vesicles. Experimentally, vesicles often assemble into multilamellar structures, so here, we determine the effect of lamellarity on sample turbidity. We find that the calculated turbidity of a 5 mM bilamellar vesicle suspension is identical to that of a 10 mM unilamellar sample (Fig. 5 *A*). More generally, for a fixed concentration of lipid (5 mM) and wavelength (400 nm), we find that the turbidity τ_q of a sample of q-bilayered vesicles is $q\times$ more than that of a unilamellar vesicle sample (Fig. 5 *A*) of turbidity τ_1: $\tau_q = q\tau_1$. A 5 mM solution of 10-bilayered vesicles will thus scatter like a 50 mM solution of unilamellar vesicles.

The strong dependence of the scattering cross section on lamellarity is a consequence of Rayleigh scattering. Because most vesicle membranes are on the order of 5 nm in thickness, the membranes behave as Rayleigh scatterers (at optical wavelengths) for which the scattering cross section σ_{sca} is proportional to m^2, the square of the scatterer's mass (35). If two membranes are in close proximity, they will scatter as a single membrane of twice the thickness and, hence, mass. The scattering cross section of a q-bilayered vesicle $\sigma_{sca,q}$ is therefore $q^2\sigma_{sca,1}$. For a fixed concentration of lipid, the number of vesicles scales inversely with the lamellarity, and so a q-bilayered sample is expected to scatter $q\times$ more than a unilamellar sample of the same concentration, leading to the same scaling seen as in our calculations (Fig. 5).

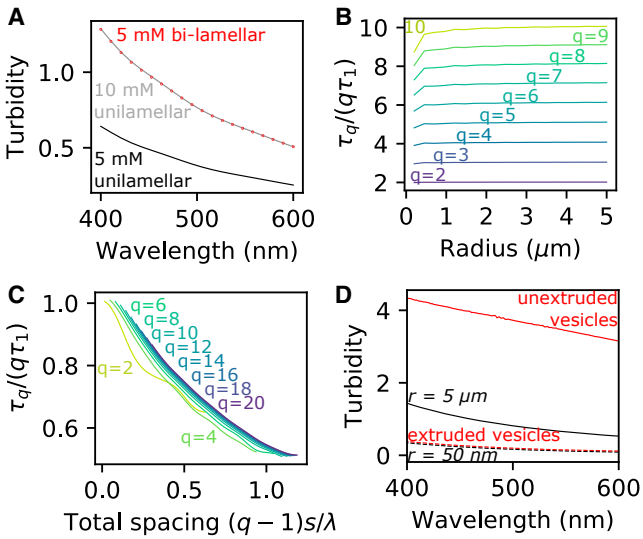

FIGURE 5 (*A*) The calculated turbidities for a 5 mM sample of bilamellar vesicles and a 10 mM sample of unilamellar vesicles are identical and twice that of a 5 mM sample of unilamellar vesicles ($r = 0.5$ μm). (*B*) The calculated turbidity of a q-bilayered sample relative to a unilamellar sample is q for a fixed concentration of amphiphile (5 mM). $\lambda = 400$ nm. (*C*) A sample's relative turbidity scales with the total spacing between the innermost and outermost membranes $(q - 1)s/\lambda$ ($r = 0.5$ μm, $\lambda = 400$ nm, $c = 5$ mM). (*D*) Experimentally measured turbidities of unextruded vesicles and vesicles extruded through 50 nm pores are shown for 5 mM oleic vesicle samples (*red lines*). Calculated turbidities are shown for 5 mM 100-nm-diameter unilamellar vesicle samples and 5 mM 10-μm-diameter unilamellar vesicle samples (*black lines*). To see this figure in color, go online.

The effect of lamellarity on scattering is weakened with increased intermembrane spacing s. For 1-μm-diameter vesicles, we find that whereas for closely spaced membranes, $\tau_q \sim q\tau_1$, the ratio $\tau_q/q\tau_1$ decreases from 1 as spacing between the innermost and outermost membranes $(q - 1)s$ increases (Fig. 5 *C*). τ_1 is the average turbidity of unilamellar vesicle samples with vesicle radii equalling that of the layers in the multilamellar vesicle. The scaling is similar regardless of the total lamellarity, which suggests that it is the distance between the innermost and outermost membranes that determines the strength of the dipole coupling.

The strong dependence of turbidity on lamellarity is surprising, and we thus seek to track the turbidity of a sample as it changes from being multilamellar to unilamellar. It is commonly noted that when a milky, heterogeneous vesicle sample is extruded through pores less than 200 nm in radius, the sample will become more transparent (22). Vesicles are large and multilamellar before extrusion and become small and predominantly unilamellar after extruding through pores smaller than 200 nm in diameter (46).

Because one of the outcomes of extrusion is to create smaller vesicles, we must attribute part of the decrease in turbidity to the size change. However, our results (Fig. 2) show that for the same concentration of lipid, the turbidity depends only logarithmically on the vesicle size. We propose that the dominant contribution to the change in vesicle turbidity during extrusion is a change in the lamellarity of the vesicles.

We find that the extruded samples scatter as expected from the calculated scattering of a sample of 100-nm-diameter unilamellar vesicles, as shown in Fig. 5 (using the wavelength-dependent refractive index of oleic acid from Jones et al. (47) for $n_{membrane}$ and wavelength-dependent refractive index of water from Engen et al. (48)). The calculated turbidity for the largest unilamellar vesicles that can occupy the volume ($r = 5$ μm) is still much smaller than the experimentally measured turbidity for unextruded vesicles, suggesting that the size of vesicles alone can not completely account for the excess scattering. Because extrusion decreases both the size and lamellarity of samples, it is highly likely that multilamellarity is responsible for the excess scattering of unextruded vesicles. For example a trilamellar sample of 5 μm vesicles would approximately have the experimentally measured turbidity. However, at such high

turbidity values, the sample is likely to be highly multiply scattering, and our simple model (Eq. 4) is no longer appropriate for direct comparisons.

Presence of inhomogeneities

We also consider cases in which an amphiphile does not form samples of vesicles that are not homogeneous. First, we consider when amphiphiles do not form membranes in solution but instead form aggregates. This can happen when the ionic strength of the solution is too high, there is precipitation (for example, divalent cations with fatty acids), the temperature is below the transition temperature of the amphiphile, or, in the case of pH-sensitive molecules, the pH is unsuitable. We model aggregates as solid spheres with $n_{\text{contents}} = n_{\text{membrane}}$.

We find that if a sample of aggregates is formed, the scattering depends nonmonotonically on wavelength and can dramatically exceed that of vesicles (Fig. 6, *A* and *B*). The nonmonotonic scaling of turbidity with aggregate size means that if the aggregates were to further aggregate, the turbidity of the sample could either increase or decrease depending on the average aggregate size.

Importantly, these results show that even a small contamination of a vesicle suspension with aggregates could dramatically change the turbidity and render such measurements useless. To mitigate the potential confusion, extrusion through small pores, sonication, and adequate mixing can all help reduce the number of aggregates present in a sample. If inhomogeneous substances, such as colloidal particles, are encapsulated, the scattering from the encapsulated material is expected to dominate the scattering from the membrane.

We also consider when samples of vesicles are inhomogeneous in size or lamellarity. We first model the turbidities of lognormal distributions of vesicles with an arithmetic mean radius of 100 nm and SDs varying from 0 nm (monodisperse sample) to 25 and 50 nm and find that the calculated turbidity does not vary by much from the monodisperse case (Fig. 6 *C*). By contrast, if a unilamellar sample of vesicles were to contain a subpopulation of bilamellar vesicles, the effect on turbidity can be quite dramatic (Fig. 6 *D*). We therefore conclude that the effect of lamellarity on turbidity can be much greater than that of vesicle size.

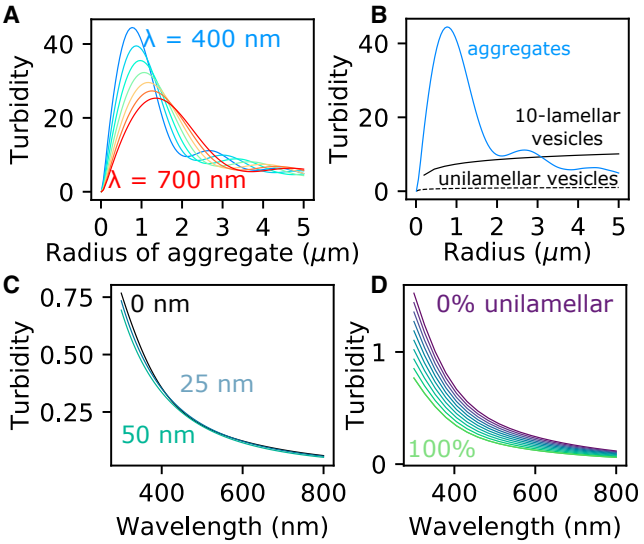

FIGURE 6 (*A*) Scattering is a nonmonotonic function of the aggregate radius, an effect that is typical of Mie scattering. For aggregates smaller than 1 μm, the scattering increases with the radius. $c = 5$ mM, $\lambda = 400$, 450, 500, 550, 600, 650, and 700 nm. (*B*) A 5 mM sample of lipid can scatter very differently depending on how the material is arranged. A sample of 1-μm-diameter aggregates scatters more than a sample of 10-bilayered vesicles, which in turn scatters more than a sample of unilamellar vesicles. $\lambda = 400$ nm. (*C*) The calculated turbidity of 5 mM samples of vesicles with mean radii 100 nm and mean SDs of 0, 25, and 50 nm do not vary much. (*D*) The calculated turbidity of vesicles varies a lot with polydispersity in lamellarity. We show calculated turbidities for 5 mM vesicle samples ($r = 100$ nm) that vary from being 100% unilamellar (0% bilamellar) to 0% unilamellar (100% bilamellar). To see this figure in color, go online.

Effects of scattering toward the detector and multiple scattering

Thus far, we have made the assumption that all of the light reaching the detector is unscattered light. However, some vesicles do scatter significantly in the forward direction (0°), and the detector is not an infinitesimal pinhole but subtends a finite angle (Fig. 7 *A*). In general, the fraction of the light f_d that passes through a circular aperture with acceptance angle $d°$ depends upon all of the vesicle parameters p. Here, we seek to determine the effect of scattering toward the detector and when that needs to be taken into account.

We calculate scattering as a function of the angle (scattering phase functions) and, in Fig. 7, *B–E*, show that vesicles larger than 100 nm in diameter scatter significantly in the forward direction. We include the fraction of scattered light that reaches detectors with acceptance angles of 1° (f_1) and 5° (f_5) as well as the asymmetry parameter $g = <\cos\theta>$, a quantity used to describe the average angle of the scattered light ($g = 1$ implies complete forward scattering, $g = -1$ implies complete backward scattering, and $g = 0$ implies isotropic scattering). In general, scatterers with a size much smaller than a tenth of the wavelength of light will scatter more isotropically; this is indeed true for the smaller vesicles (Fig. 7). Conversely, scatterers that are much larger tend to scatter more light forward (35).

To quantify how much extra light is reaching the detector because of forward scattering, we consider two models. The first one models single scattering with the exact phase function, and the second one models multiple scattering using an approximation of the phase function (34).

When considering singly scattering samples, the intensity of light reaching a detector in the absence of absorption and forward scattering is $I = I_0 e^{-\tau}$. The amount of light that is scattered to a detector that has a circular aperture with acceptance angle $d°$ accepting a fraction of the light f_d is

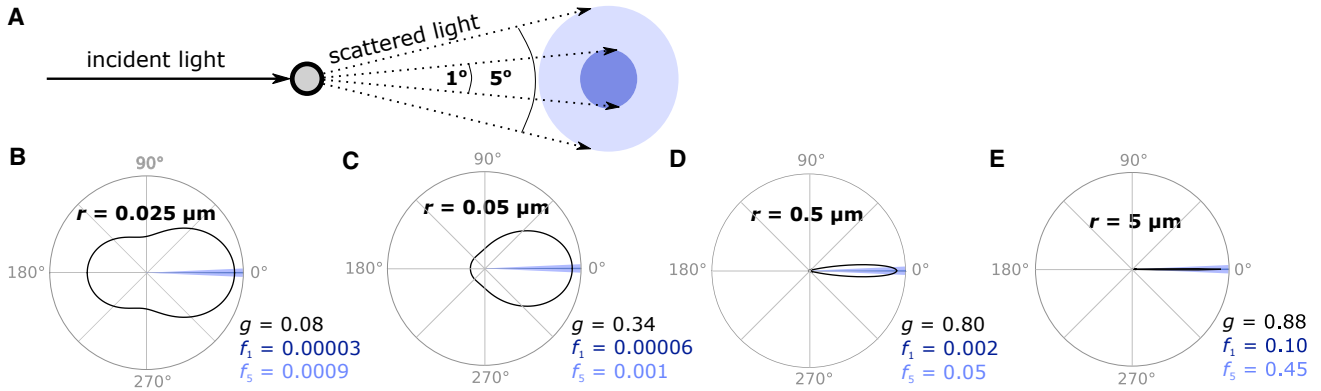

FIGURE 7 (*A*) Vesicles that scatter forward can scatter light toward a detector. The fraction of scattered light reaching the detector depends on the detector size. (*B–E*) The intensity of light scattered as a function of angle is shown on polar plots, and the asymmetry parameter g and the fraction of scattered light reaching detectors with circular apertures subtending 1° (f_1) and 5° (f_5) are shown. Calculations are done for four different vesicle sizes. Larger vesicles scatter more in the forward direction. $\lambda = 400$ nm. To see this figure in color, go online.

$$f_d I_s = f_d(I_0 - I) = f_d\left(I_0 - I_0 e^{-\tau}\right) = f_d I_0\left(1 - e^{-\tau}\right). \quad (7)$$

The amount of light I_{obs} observed by the detector, including unscattered light, is hence

$$\begin{aligned} I_{\text{obs}} &= I_0 e^{-\tau} + f_d I_s = I_0 e^{-\tau} + f_d I_0\left(1 - e^{-\tau}\right) \\ &= I_0\left(f_d + (1 - f_d)e^{-\tau}\right). \end{aligned} \quad (8)$$

The observed turbidity τ_{obs} is thus

$$\tau_{\text{obs}} = -\ln(I_{\text{obs}}/I_0) = -\ln\left(f_d + (1 - f_d)e^{-\tau}\right). \quad (9)$$

We can therefore use Eq. 9 to understand how much the turbidity detected on a spectrophotometer τ_{obs} underestimates the true turbidity τ as a result of forward scattering. We plot τ_{obs}/τ in Fig. 8 as a function of f_d and τ, with the four vesicle types in Fig. 7, *B–E* overlaid. As expected, the experimentally observed τ_{obs} is approximately equal to τ for smaller vesicles because they scatter less strongly in the forward direction, but the disagreement between τ_{obs} and τ grows with increasing d and f_d. Because τ_{obs}/τ depends on the acceptance angle d and hence the geometry of the spectrophotometer, it may be difficult to directly compare measurements made on different spectrophotometers. Spectrophotometers are thus suitable for quantifying the turbidity of samples of smaller vesicles; measurements of samples of larger vesicles can severely underestimate τ because of forward scattering, unless the acceptance angle d is very small.

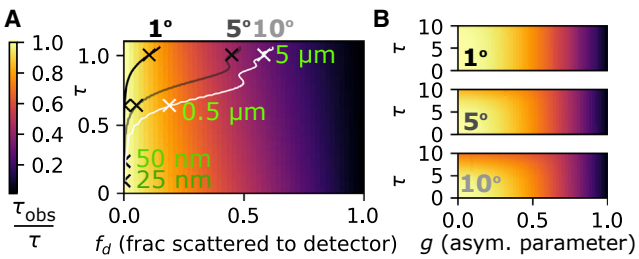

FIGURE 8 (*A*) τ_{obs}/τ is plotted as a function of f_d and τ, assuming no scattering in the direction of the detector. The f_d and τ for 1° (*black*), 5° (*gray*), and 10° (*white*) circular apertures are shown for 5 mM samples of vesicles with different radii. A 5 mM sample of the vesicles from Fig. 7, *B–E* are marked with crosses (radii in *green*). $\lambda = 400$ nm. (*B*) τ_{obs}/τ is plotted as a function of g and τ for 1°, 5°, and 10° circular apertures. To see this figure in color, go online.

We now seek to determine the effect of multiple scattering on the measured turbidity τ_{obs}. Numerical methods are often required to accurately model radiative transfer. To gain some understanding of the effects of multiple scattering without creating a full numerical simulation, we use a model from atmospheric sciences (33) to calculate how much light reaches an aperture—the detector—after passing through turbid media. This model is more accurate than Eq. 4 for large τ but approximates the phase function (34). We find that even for small scatterers ($g \sim 0$), τ_{obs}/τ can decrease from unity (Fig. 8 *B*) if the sample is concentrated enough. Again, τ_{obs}/τ depends on the geometry of the instrument. For further discussions of multiple scattering, we refer the reader to articles that provide accessible overviews of the relevant concepts (49–51).

Implications for experimental design

We have shown how the measured turbidity of a sample depends on the amphiphile concentration c, path length l, and $\{p\} = \{r_i, n_{\text{contents}}, t, n_{\text{membrane}}\}$, summarized in Table 1. To measure any one parameter with a spectrophotometer, one must control for all of the others. We have also shown the limitations of using spectrophotometers to measure turbidity, with the simplest results to interpret being the results for a dilute sample of small vesicles. We now illustrate how turbidity can be used in conjunction with other tools to gauge information about experimental samples.

TABLE 1 Summary of How τ Scales with Different Parameters

Parameter	Explanation	Scaling
r	vesicle radius	~logarithmic
$t\Delta n$	optical path difference	quadratic
Δn_{io} or k	content/medium index contrast	~quadratic
k	absorbing contents	~quadratic
q	lamellarity	linear
c	concentration	linear
l	path length of light	linear

Application 1. Interpreting turbidity measurements during vesicle formation

During de novo vesicle formation that is triggered by a drop in pH, turbidity can be used to monitor the assembly of vesicles from micelles. In brief, a solution of micelles at a high pH is added to a solution buffered at a pH near the pKa of the fatty acids. At this lower pH, vesicles are thermodynamically favored over micelles. A commonly used assumption is that any increase in scattering of the solutions is because of the fatty acids rearranging into vesicles and scattering more light. The turbidity of the sample is hence expected to increase over time.

Upon adding a solution of oleic acid micelles to 50 mM bicine (pH 8.1) to a final oleic acid concentration of 5 mM, we find that the turbidity changes nonmonotonically with time (Fig. 9). The sample turbidity initially increases to a maximum one day after the sample is first made and then decreases during the second day. The decrease in turbidity is at first glance surprising because the number, lamellarity, or size of vesicles is not expected to decrease with time. All other parameters p are constant during the experiment.

By monitoring the samples with phase-contrast microscopy, we were able to determine that at one day, the sample consists mostly of highly scattering nonspherical aggregates or extremely multilamellar, nonspherical vesicles with little encapsulation volume (Fig. 9). Because the size of the oleic acid structures increases from small aggregates to large oligolamellar vesicles, the decrease in turbidity cannot be attributed to a decrease in vesicle size. From the phase-contrast images, we can see that for the same concentration of lipid, aggregates and very multilamellar vesicles can scatter a lot more light than oligolamellar vesicles. We therefore attribute the decrease in turbidity to the aggregates disappearing and giant oligolamellar vesicles forming in their place.

Application 2. Measuring membrane thickness with turbidity

We measure the membrane thickness of oleic acid vesicles by fitting a model containing information about all of the parameters p except the thickness t to measured sample turbidity. We use the wavelength-dependent refractive index of oleic acid from Jones et al. (47) for $n_{membrane}$ and wavelength-dependent refractive index of water from Engen et al. (48). To control for size and lamellarity, we extrude vesicles through 50-nm-diameter pores to achieve an almost completely unilamellar sample (46). We model the distributions as lognormal using the arithmetic means and SDs determined with DLS (Malvern Zetasizer Nano C). For the samples shown in Fig. 9 *B*, $2r = 124 \pm 42$ nm for oleic acid, $2r = 109 \pm 37$ nm for palmitoleic acid, and $2r = 86 \pm 30$ nm for myristoleic acid. The scattering cross sections for different vesicle radii are weighted by the size distribution and added together to calculate the sample turbidity. Examples for how to use our code can be found at https://github.com/anna-wang/vesicle-turbidity.

Our model fits the data at all wavelengths extremely well. Keeping all other parameters fixed, we use a Levenberg-Marquardt-based least-squares algorithm to find the best fit thickness for oleic acid: 3.2 nm (SD 0.1 nm, number of samples $n = 4$). This is in good agreement with transmission

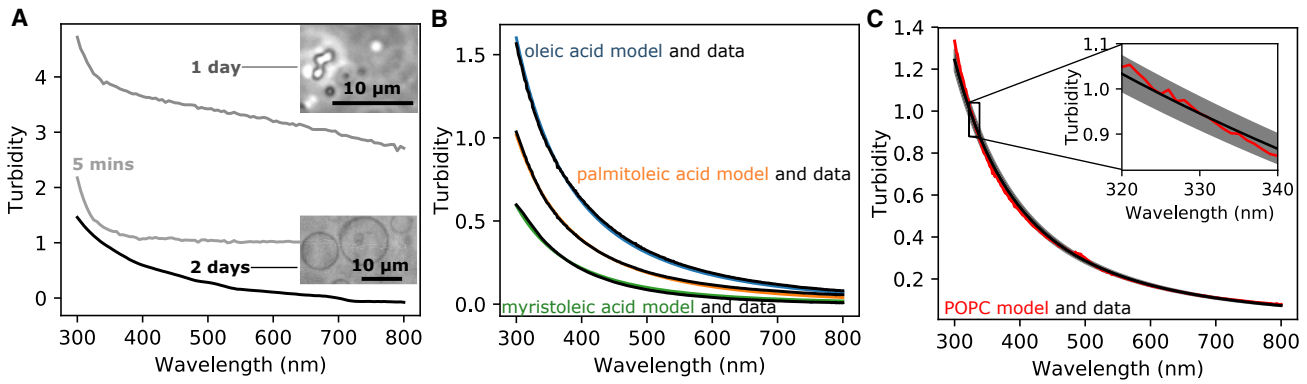

FIGURE 9 (*A*) A 5 mM oleic acid sample (50 mM bicine (pH 8.1)) is highly scattering after one day but becomes more translucent by day two. Examining the sample with phase-contrast microscopy reveals that the sample transitions from being mostly aggregates to mostly oligolamellar. (*B*) The turbidity of oleic acid (*blue*), palmitioleic acid (*orange*), and myristoleic acid (*green*) vesicles after extrusion are fitted well by a model that takes into account the size distributions, concentration, and vesicle composition. The buffer is 200 mM bicine (pH 8.1) for all samples. The concentration of lipids partitioned into the vesicle phase is 8.26 mM minus the critical vesicle concentration from Budin et al. (57). (*C*) A model (*black*) for 5-nm-thick membranes fits the turbidity of an extruded 1 mM POPC vesicle sample (*red*) well. The modeled turbidities of 4.9-nm-thick to 5.1-nm-thick membranes are shown in gray, which are more visible in the inset. To see this figure in color, go online.

electron cryomicroscopy measurements by Namani et al. (52) (3.6 ± 0.8 nm) and simulations by Han (38) (2.75–3.5 nm). Assuming that at all wavelengths $n_{\text{oliec}} - n_{\text{palmitoleic}} < 0.01$ and $n_{\text{palmitoleic}} - n_{\text{myristoleic}} < 0.01$, the thickness of palmitoleic acid/palmitoleate and myristoleic acid/myristoleate membranes are 2.7–2.9 nm and 2.5–2.7 nm. We show the best fit thickness results for three vesicle samples in Fig. 9 *B*.

We adopt the same strategy to measure the thickness of POPC membranes, using the wavelength-dependent refractive index for egg-phosphatidylcholine from Khlebtsov et al. (53) and the area per lipid from Kucerka et al. (54). The vesicle size measured by DLS for the POPC sample shown in Fig. 9 *C* is $2r = 162 \pm 54$ nm. We find that the best fit thickness for our POPC samples is 4.9 nm (SD 0.1 nm, number of samples $n = 4$) in good agreement with the measured steric bilayer thickness values from Huber et al. (55) and Leftin et al. (56).

For both oleic acid vesicles and POPC vesicles, our best-fit thickness model reproduces the experimental results extremely well at all wavelengths. These results clearly demonstrate that measurements of vesicle parameters can be made if the other parameters can be constrained.

DISCUSSION

We have shown that an extended Lorenz-Mie model for core-shell scatterers can be used to effectively model light scattering by vesicles. Our calculations show the turbidity of a vesicle solution depends on the presence of encapsulated contents, aggregates, and multilamellar vesicles. Turbidity measurements are thus complicated to interpret, and it may not be possible to generalize the results enough in a single article so that experimenters can always interpret turbidity measurements in a straightforward manner. However, we attempt to show how quantitative interpretations can be made.

Because the turbidity depends on so many parameters, tools other than a spectrophotometer must be used to understand which parameters are contributing. For instance, the calculated turbidity for a sample of bilamellar vesicles is identical to the turbidity of a sample of unilamellar vesicles with twice the lipid concentration. As a further example, it may have been tempting to interpret the high turbidity of the sample in Fig. 9 at day one as the presence of a high concentration of vesicles. We reveal that, in fact, the high turbidity was because of a high concentration of aggregates and that, seemingly paradoxically, the number of vesicles increases only when the turbidity drops. In this particular case, we were able to use microscopy to correctly interpret the turbidity measurements.

Our model enables more accurate modeling of turbidimetric measurements than the Rayleigh-Gans-Debye approximation. Even so, the observed (τ_{obs}) and modeled (τ) turbidity begin to differ significantly when forward and multiple scattering become significant. We provide guidelines for when interpreting turbidity data in a quantitative manner becomes difficult owing to these reasons. We note that the dependence of τ_{obs} on the detector acceptance angle d means that this effect is instrument dependent. Thus, the knowledge of the exact light path within the spectrophotometer is required to make a complete model and overcome these limitations.

We also showed that, with careful experimental design, turbidity can be quite a powerful tool. By using extrusion to constrain lamellarity and DLS to measure the vesicle size distribution, we were able to model how such a vesicle sample would scatter light to measure the membrane thickness of oleic acid vesicles and POPC vesicles. Our results are in agreement with values in literature, but instead of requiring manual measurements on a transmission electron cryomicroscopy, our method uses equipment easily accessible to those that work routinely with vesicles—an extruder, a DLS instrument, a spectrophotometer, and a computer.

We hope that our results for how the turbidity of a vesicle sample changes with lipid refractive index, encapsulated contents, vesicle size, lipid membrane thickness, and lamellarity can be used as an aid for researchers when interpreting their turbidity measurements and understanding how the exact material configuration and distribution within a vesicle affects its interaction with light.

AUTHOR CONTRIBUTIONS

A.W. and J.W.S. conceived of the article. A.W. and C.C.M. designed and performed the simulations, and A.W. designed and carried out the experiments and associated analyses. A.W., C.C.M., and J.W.S. wrote the manuscript.

ACKNOWLEDGMENTS

We thank Dr. Lijun Zhou for the oligomers used for the refractive index measurements, Dr. Derek O'Flaherty for helpful discussions and reading of the article, and Dr. Daniel Duzdevich, Dr. Li Li, Travis Walton, and Dr. Victor Lelyveld for feedback on the article. J.W.S. is an Investigator of the Howard Hughes Medical Institute.

This work was supported in part by a grant from the Simons Foundation (290363) to J.W.S. A.W. was supported by an appointment to the National Aeronautics and Space Administration Postdoctoral Program, administered by Universities Space Research Association under contract with NASA.

REFERENCES

1. Bozzuto, G., and A. Molinari. 2015. Liposomes as nanomedical devices. *Int. J. Nanomedicine*. 10:975–999.
2. Patel, D., C. Patel, and R. Jani. 2011. Ufasomes: a vesicular drug delivery. *Systematic Reviews in Pharmacy*. 2:72.
3. Schwille, P., and S. Diez. 2009. Synthetic biology of minimal systems. *Crit. Rev. Biochem. Mol. Biol.* 44:223–242.
4. Deamer, D. 2017. The role of lipid membranes in life's origin. *Life (Basel)*. 7:5.

5. Tahara, K., S. Tadokoro, …, N. Hirashima. 2012. Endocytosis-like uptake of surface-modified drug nanocarriers into giant unilamellar vesicles. *Langmuir.* 28:7114–7118.
6. Egelhaaf, S. U., E. Wehrli, …, P. Schurtenberger. 1996. Determination of the size distribution of lecithin liposomes: a comparative study using freeze fracture, cryoelectron microscopy and dynamic light scattering. *J. Microsc.* 184:214–228.
7. Morigaki, K., and P. Walde. 2002. Giant vesicle formation from oleic acid/sodium oleate on glass surfaces induced by adsorbed hydrocarbon molecules. *Langmuir.* 18:10509–10511.
8. Van Zanten, J. H., and H. G. Monbouquette. 1991. Characterization of vesicles by classical light scattering. *J. Colloid Interface Sci.* 146:330–336.
9. Kamentsky, L. A., M. R. Melamed, and H. Derman. 1965. Spectrophotometer: new instrument for ultrarapid cell analysis. *Science.* 150:630–631.
10. Were, L. M., B. D. Bruce, …, J. Weiss. 2003. Size, stability, and entrapment efficiency of phospholipid nanocapsules containing polypeptide antimicrobials. *J. Agric. Food Chem.* 51:8073–8079.
11. Hanczyc, M. M., S. M. Fujikawa, and J. W. Szostak. 2003. Experimental models of primitive cellular compartments: encapsulation, growth, and division. *Science.* 302:618–622.
12. Hanczyc, M. M., S. S. Mansy, and J. W. Szostak. 2007. Mineral surface directed membrane assembly. *Orig. Life Evol. Biosph.* 37:67–82.
13. Sahai, N., H. Kaddour, …, M. Gao. 2017. Mineral surface chemistry and nanoparticle-aggregation control membrane self-assembly. *Sci. Rep.* 7:43418.
14. Wang, L., C. Quan, …, S. Fan. 2013. Functional reconstitution of *Staphylococcus aureus* truncated AgrC histidine kinase in a model membrane system. *PLoS One.* 8:e80400.
15. Cohen, B. E., and A. D. Bangham. 1972. Diffusion of small non-electrolytes across liposome membranes. *Nature.* 236:173–174.
16. Black, R. A., M. C. Blosser, …, S. L. Keller. 2013. Nucleobases bind to and stabilize aggregates of a prebiotic amphiphile, providing a viable mechanism for the emergence of protocells. *Proc. Natl. Acad. Sci. USA.* 110:13272–13276.
17. Chong, C. S., and K. Colbow. 1976. Light scattering and turbidity measurements on lipid vesicles. *Biochim. Biophys. Acta.* 436:260–282.
18. Elsayed, M. M., and G. Cevc. 2011. Turbidity spectroscopy for characterization of submicroscopic drug carriers, such as nanoparticles and lipid vesicles: size determination. *Pharm. Res.* 28:2204–2222.
19. Matsuzaki, K., O. Murase, …, S. Kobayashi. 2000. Optical characterization of liposomes by right angle light scattering and turbidity measurement. *Biochim. Biophys. Acta.* 1467:219–226.
20. Bezrukova, A. G., and O. A. Rozenberg. 1981. Determination of the parameters of liposomes by the turbidity spectrum method. *Bull. Exp. Biol. Med.* 91:553–555.
21. Khlebtsov, N. G., L. A. Kovler, …, V. A. Bogatyrev. 2001. Spectroturbidimetry of liposome suspensions. *Colloid J.* 63:491–498.
22. Avanti Polar Lipids Inc. Mini-Extruder Extrusion Technique. https://avantilipids.com/divisions/equipment-products/mini-extruder-extrusion-technique.
23. Yoshikawa, W., H. Akutsu, and Y. Kyogoku. 1983. Light-scattering properties of osmotically active liposomes. *Biochim. Biophy. Acta.* 735:397–406.
24. Walstra, P. 1964. Approximation formulae for the light scattering coefficient of dielectric spheres. *Br. J. Appl. Phys.* 15:1545–1552.
25. Yang, W. 2003. Improved recursive algorithm for light scattering by a multilayered sphere. *Appl. Opt.* 42:1710–1720.
26. Barkley, S., T. G. Dimiduk, …, A. Wang. 2018. Holographic microscopy with Python and HoloPy. *ArXiv*, arXiv:1806.00058 https://arxiv.org/abs/1806.00058.
27. Aden, A. L., and M. Kerker. 1951. Scattering of electromagnetic waves from two concentric spheres. *J. Appl. Phys.* 22:1242–1246.
28. Rosoff, M. 1996. Vesicles. CRC Press, Boca Raton, FL.
29. Suzuki, H., and I.-Y. Sandy Lee. 2013. Mie scattering field inside and near a coated sphere: computation and biomedical applications. *J. Quant. Spectrosc. Radiat. Transf.* 126:56–60.
30. Moosmüller, H., R. K. Chakrabarty, and W. P. Arnott. 2009. Aerosol light absorption and its measurement: a review. *J. Quant. Spectrosc. Radiat. Transf.* 110:844–878.
31. Averitt, R. D., D. Sarkar, and N. J. Halas. 1997. Plasmon resonance shifts of Au-coated ${\mathrm{Au}}_{2}S$ nanoshells: insight into multicomponent nanoparticle growth. *Phys. Rev. Lett.* 78:4217–4220.
32. Oldenburg, S. J., R. D. Averitt, …, N. J. Halas. 1998. Nanoengineering of optical resonances. *Chem. Phys. Lett.* 288:243–247.
33. Shettle, E. P., and J. A. Weinman. 1970. The transfer of solar irradiance through inhomogeneous turbid atmospheres evaluated by Eddington's approximation. *J. Atmos. Sci.* 27:1048–1055.
34. Joseph, J. H., W. J. Wiscombe, and J. A. Weinman. 1976. The delta-Eddington approximation for radiative flux transfer. *J. Atmos. Sci.* 33:2452–2459.
35. Bohren, C. F., and D. R. Huffman. 1998. Absorption and Scattering of Light by Small Particles. Wiley-VCH, New York.
36. Yurkin, M. A., and A. G. Hoekstra. 2011. The discrete-dipole-approximation code ADDA: capabilities and known limitations. *J. Quant. Spectrosc. Radiat. Transf.* 112:2234–2247.
37. Wang, A., T. G. Dimiduk, …, V. N. Manoharan. 2014. Using the discrete dipole approximation and holographic microscopy to measure rotational dynamics of non-spherical colloidal particles. *J. Quant. Spectrosc. Radiat. Transf.* 146:499–509.
38. Han, S. 2013. Molecular dynamics simulation of oleic acid/oleate bilayers: an atomistic model for a ufasome membrane. *Chem. Phys. Lipids.* 175–176:79–83.
39. Hargreaves, W. R., and D. W. Deamer. 1978. Liposomes from ionic, single-chain amphiphiles. *Biochemistry.* 17:3759–3768.
40. Jin, L., A. E. Engelhart, …, J. W. Szostak. 2018. Preparation, purification, and use of fatty acid-containing liposomes. *J. Vis. Exp.* 132:e57324.
41. Sunami, T., F. Caschera, …, T. Yomo. 2010. Detection of association and fusion of giant vesicles using a fluorescence-activated cell sorter. *Langmuir.* 26:15098–15103.
42. Castanho, M. R. B., N. C. Santos, and L. M. S. Loura. 1997. Separating the turbidity spectra of vesicles from the absorption spectra of membrane probes and other chromophores. *Eur. Biophys. J.* 26:253–259.
43. Plass, G. N. 1966. Mie scattering and absorption cross sections for absorbing particles. *Appl. Opt.* 5:279–285.
44. Nadeau, J. L., Y. B. Cho, and C. A. Lindensmith. 2015. Use of dyes to increase phase contrast for biological holographic microscopy. *Opt. Lett.* 40:4114–4117.
45. AAT Bioquest. Search molar extinction coefficient (ε). https://www.aatbio.com/resources/extinction-coefficient/.
46. Mayer, L. D., M. J. Hope, and P. R. Cullis. 1986. Vesicles of variable sizes produced by a rapid extrusion procedure. *Biochim. Biophys. Acta.* 858:161–168.
47. Jones, S. H., M. D. King, and A. D. Ward. 2015. Atmospherically relevant core-shell aerosol studied using optical trapping and Mie scattering. *Chem. Commun. (Camb.).* 51:4914–4917.
48. Van Engen, A. G., S. A. Diddams, and T. S. Clement. 1998. Dispersion measurements of water with white-light interferometry. *Appl. Opt.* 37:5679–5686.
49. Walstra, P. 1965. Discussion of errors in turbidimetry. *Br. J. Appl. Phys.* 16:1187–1192.
50. Rogers, W. B., M. Corbett, …, V. N. Manoharan. 2014. Breaking tradeoffs between translucency and diffusion in particle-doped films. *Opt. Mater. Express.* 4:2621–2631.
51. Small, A., S. Hong, and D. Pine. 2005. Scattering properties of core–shell particles in plastic matrices. *J. Polym. Sci. B. Polym. Phys.* 43:3534–3548.

52. Namani, T., T. Ishikawa, …, P. Walde. 2007. Vesicles from docosahexaenoic acid. *Colloids Surf. B Biointerfaces.* 54:118–123.

53. Khlebtsov, B., L. Kovler, …, S. Shchyogolev. 2003. Studies of phosphatidylcholine vesicles by spectroturbidimetric and dynamic light scattering methods. *J. Quant. Spectrosc. Radiat. Transf.* 79–80:825–838.

54. Kučerka, N., M. P. Nieh, and J. Katsaras. 2011. Fluid phase lipid areas and bilayer thicknesses of commonly used phosphatidylcholines as a function of temperature. *Biochim. Biophys. Acta.* 1808:2761–2771.

55. Huber, T., K. Rajamoorthi, …, M. F. Brown. 2002. Structure of docosahexaenoic acid-containing phospholipid bilayers as studied by (2)H NMR and molecular dynamics simulations. *J. Am. Chem. Soc.* 124:298–309.

56. Leftin, A., T. R. Molugu, …, M. F. Brown. 2014. Area per lipid and cholesterol interactions in membranes from separated local-field (13) C NMR spectroscopy. *Biophys. J.* 107:2274–2286.

57. Budin, I., N. Prwyes, …, J. W. Szostak. 2014. Chain-length heterogeneity allows for the assembly of fatty acid vesicles in dilute solutions. *Biophys. J.* 107:1582–1590.